Materials Science & Engineering A 649 (2016) 123–127

Contents lists available at ScienceDirect

Materials Science & Engineering A

journal homepage: www.elsevier.com/locate/msea

Short communication

On the contributions of different micromechanisms for enhancement in the strength of TI–6Al–4V alloy upon B addition: A nanomechanical analysis

Moo-Young Seok [a], Yakai Zhao [a], Jung-A Lee [a], Reda M. Mohamed [b], Laila M. Al-Harbi [b], Mohammed S. Al-Ghamdi [c], Gaurav Singh [d], Upadrasta Ramamurty [d,e,*], Jae-il Jang [a,**]

[a] Division of Materials Science and Engineering, Hanyang University, Seoul 133-791, Republic of Korea
[b] Chemistry Department, Faculty of Science, King Abdulaziz University, PO Box 80203, Jeddah 21589, Saudi Arabia
[c] Physics Department, Faculty of Science, King Abdulaziz University, PO Box 80203, Jeddah 21589, Saudi Arabia
[d] Department of Materials Engineering, Indian Institute of Science, Bangalore 560012, India
[e] Center of Excellence for Advanced Materials Research, King Abdulaziz University, Jeddah 21589, Saudi Arabia

ARTICLE INFO

Article history:
Received 16 August 2015
Received in revised form
25 September 2015
Accepted 26 September 2015
Available online 30 September 2015

Keywords:
Ti alloys
Nanoindentation
Strengthening
Hardness
Slip lines

ABSTRACT

The addition of small amount of boron to Ti and it alloys refines the as-cast microstructure and enhances the mechanical properties. In this paper, we employ nanoindentation on each of the constituent phases in the microstructure and 'rule-of-mixture' type analysis to examine their relative contributions to the strength enhancement in a Ti–6Al–4V alloy modified with 0.3 wt% B. Our results indicate to two main contributors to the relatively higher flow strength of B-modified alloy vis-á-vis the base alloy: (a) strengthening of alpha phase due to the reduction in the effective slip length that occurs as a result of the microstructural refinement that occurs upon B addition, and (b) composite strengthening caused by the TiB whiskers present in the alloy.

© 2015 Elsevier B.V. All rights reserved.

1. Introduction

Titanium (Ti) and its alloys are widely used in various aerospace and non-aerospace industries due to their very high specific strength and stiffness combined with excellent corrosion and oxidation resistances over wide temperature range [1,2]. Amongst various Ti alloys, Ti–6Al–4V (hereafter referred to as Ti64) is the most popular and constitutes more than 50% of total Ti usage. Its typical microstructure in mill-annealed condition consists of alternate layers of hexagonal close packed (hcp) α and body centered cubic (bcc) β phases, which are related through the Burgers orientation relationship [3]. The mechanical properties of Ti64 alloy strongly depend upon its microstructural parameters like prior β grain size, α-β colony size, α lath thickness, and volume fractions of α and β phases [4,5].

Generally, the microstructures of Ti64 alloy in the as-cast condition tend to be coarse, with prior β grain size in the order of several millimeters [6]. This necessitates considerable thermo-mechanical processing of the alloy either in the β or $\alpha+\beta$ phase field to break the as-cast structure down, which in turn, makes the finished components expensive. Recently, it has been shown that trace additions of B in Ti64 alloy refine its grain-size by more than an order of magnitude [7,8], which can potentially reduce the processing steps required. Consequently, the mechanical behavior of B-modified Ti64 alloys are widely researched [8–14]. An outstanding question that remains unanswered in the context of the strength enhancement due to B-addition is the following: "Is it primarily due to microstructure refinement or due to the enhancement of the flow strengths of the constituent phases, particularly that of the α phase?" In trying to address this issue, we employ the nanoindentation technique to analyze the strength of each the constituent phase in B-free and 0.3 wt% B added Ti64, and critically examine the different mechanisms contributions to the overall strength enhancement.

2. Materials and experiments

Two alloys (Ti64 and Ti64-0.3 wt% B, which will be referred as Ti64-B hereafter), both in the as-cast condition, were investigated

* Corresponding author at: Indian Institute of Science, Bangalore 560012, India.
** Corresponding author at: Hanyang University, Seoul 133-791, Republic of Korea.
E-mail addresses: ramu@materials.iisc.ernet.in (U. Ramamurty), jijang@hanyang.ac.kr (J.-i. Jang).

http://dx.doi.org/10.1016/j.msea.2015.09.103
0921-5093/© 2015 Elsevier B.V. All rights reserved.

in this work. The alloys were induction skull melted and subsequently hot-isostatic pressed (HIPed) at 900 °C under 100 MPa pressure for 2 h. Further details pertaining to effect of B additions on the microstructure and mechanical response of Ti64 can be found in the work of Sen et al. [8,9]. Nanoindentation experiments were conducted to evaluate the hardness, H, of individual α and β phases. For this purpose, specimens with size $10 \times 10 \times 2$ mm^3 were metallographically prepared to mirror finish using standard grinding and polishing procedures. To avoid artifacts related to a possible hardened surface layer, polished specimens were then electropolished in a solution of 93% CH_3OH + 7% H_2SO_4 using Lectropol-5 instrument (Struers, Westlake, OH). Specimens were etched with Kroll's reagent (5% HF + 10% HNO_3 + 85% distilled water) for microstructure observations with a scanning electron microscopy (SEM), Nova NanoSEM 450 (FEI, Hillsboro, OR). Volume fraction of each phase was measured by an image analyzer, Image-Pro (Media Cybernetics Inc., Silver Spring, MD). The nanoindentation tests were carried out at room temperature using the continuous stiffness measurement (CSM) module of the Nanoindenter-XP (formerly MTS; now Keysight Technologies, Oak Ridge, TN) with a Berkovich tip, at a constant indentation strain rate ($dP/dt)/P$ (where P is the indentation load) of 0.05/s. The values of H were estimated according to the Oliver–Pharr method [15]. Uniaxial stress–strain responses were measured, in both tensile and compressive mode at room temperature, with a nominal strain rate of 8.33×10^{-5}/s. Tensile tests were conducted on plate-type specimens (with 6 mm width, 15 mm gage length, and 2 mm thickness) using an MTS Sintech 5/G machine (MTS., Eden Prairi, MN), while compression tests were conducted on cylindrical specimens (with 4 mm diameter and 8 mm height) using an MTS Criterion machine. During compression test, strain was measured with a laser extensometer, MTS LX-500.

3. Results and discussion

Fig. 1(a) and (b) show representative SEM micrographs of Ti64 and Ti64-B alloys, respectively. The phase contrast in these micrographs is α: dark gray; β: bright gray, and TiB: white.

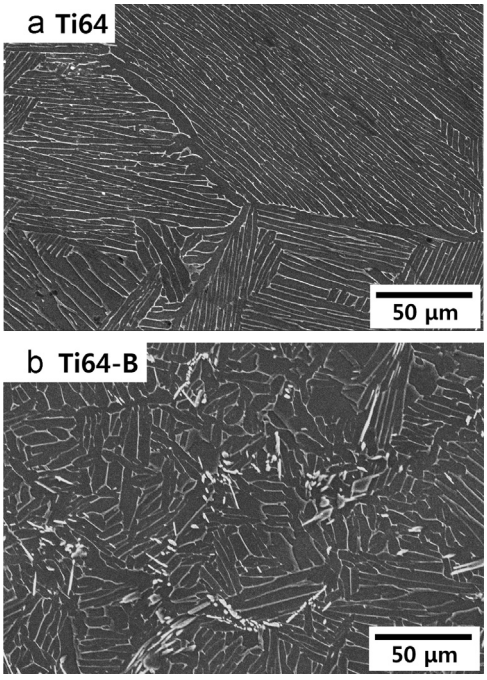

Fig. 1. Representative SEM images of (a) Ti–6Al–4V and (b) Ti–6Al–4V–0.3B.

Table 1
Microstructural parameters like prior β grain size (d), α-β colony size (c), α lath size (λ), volume fractions of α and β (f_α, f_β) and TiB particles (f_{TiB}) in Ti64 and Ti64-B alloys. Data of d, c, λ are taken from Ref. [9].

Alloy	d (μm)	c (μm)	λ (μm)	f_α	f_β	f_{TiB}
Ti64	2386.2 ± 871	244.4 ± 51.1	2.5 ± 0.9	~0.88	~0.12	0
Ti64-B	121.1 ± 27.6	23.7 ± 6.6	4.7 ± 1.3	~0.88	~0.10	~0.02

Microstructure consists of α-β colony structure with alternate layers of α and thin β phases. The α-β laths are oriented along preferred orientations to form colonies which are randomly oriented within a single prior-β grain. Microstructural parameters like prior β grain size, d, α-β colony size, c, α lath size, λ, volume fractions of α and TiB phases, f_α, f_{TiB}, which were measured and reported in Ref. [9], are listed in Table 1. As evident from Fig. 1 (b) and Table 1, addition of 0.3 wt% B in Ti64 reduces d and c dramatically by more than an order of magnitude. However, λ increases from 2.5 μm in Ti64 to 4.7 μm in Ti64-B alloy, which is controlled by cooling rate during solidification [7]. Further, TiB precipitates (white in Fig. 1b), located at the prior β grain boundaries in the form of whiskers having aspect ratio of ~9–10, can be seen, with f_{TiB} of ~2% [9].

Representative tensile and compression stress–strain responses are displayed in Fig. 2a. The yield and flow stress of B-modified alloy are higher than the B-free Ti64, confirming that the small addition of B indeed enhances the strength of Ti64, with a maximum enhancement in the flow stress, $\Delta\sigma$, of ~120 MPa, which is consistent with that reported by Sen et al. [9]. Importantly, a significant tension–compression asymmetry (TCA) in yield strength, σ_y, is noted, i.e., σ_y in compression is higher than σ_y in tension. In α+β Ti alloys such as Ti64, TCA arises due to back-stress generation due to dislocation pile-up at the α-β interfaces [16]. Since our objective is to compare the uniaxial responses with those of indentation, and the state of stress in the latter is predominantly compressive in nature, we will use only the compression data from here onwards in this paper.

Microstructural examination of the compression tested samples indicate that in Ti64, slip lines (as marked as white dashed lines in Fig. 2b) cut across several α-β interfaces. In Ti64-B on the contrary, no such features could be seen (Fig. 2c). It is well known that planar slip prevails in α-Ti in view of the limited number of independent slip systems in the hcp crystal structure [17–19]. Such planar slip could lead to shearing across the α-β interfaces that are crystallographically related, as seen in Fig. 2b. However, it did not occur in Fig. 2c, from which it was believed that the effective slip length becomes apparently shorter in Ti64-B. One can imagine that much less cutting behavior can be the results from the stronger β phase in Ti64-B. However, as will be shown later, there is negligible difference in β phase hardness between Ti64 and Ti64-B. Thus, although it is not fully understood at this point, it is reasonable to assume that the less cutting behavior (and thus the apparent reduction in effective slip length) is closely related to the reduction in the α-β colony size, c, which is major change in microstructure with B addition. Note that, in Ti64, the colony size is known to set the effective slip length for deformation [9]. Indeed, earlier work, where B content in Ti64 and in turn microstructural length scales were systematically varied, has clearly established that the Hall-Petch relation is obeyed when σ_y is plotted against c [9]. Thus, the addition of B to Ti64, which reduces the colony size considerably, causes a marked reduction in the effective slip length. This, in turn, constrains the plastic deformation within a colony and hence increasing the strength of Ti64 upon the addition of B.

Fig. 3 shows typical load-displacement (P–h) curves recorded

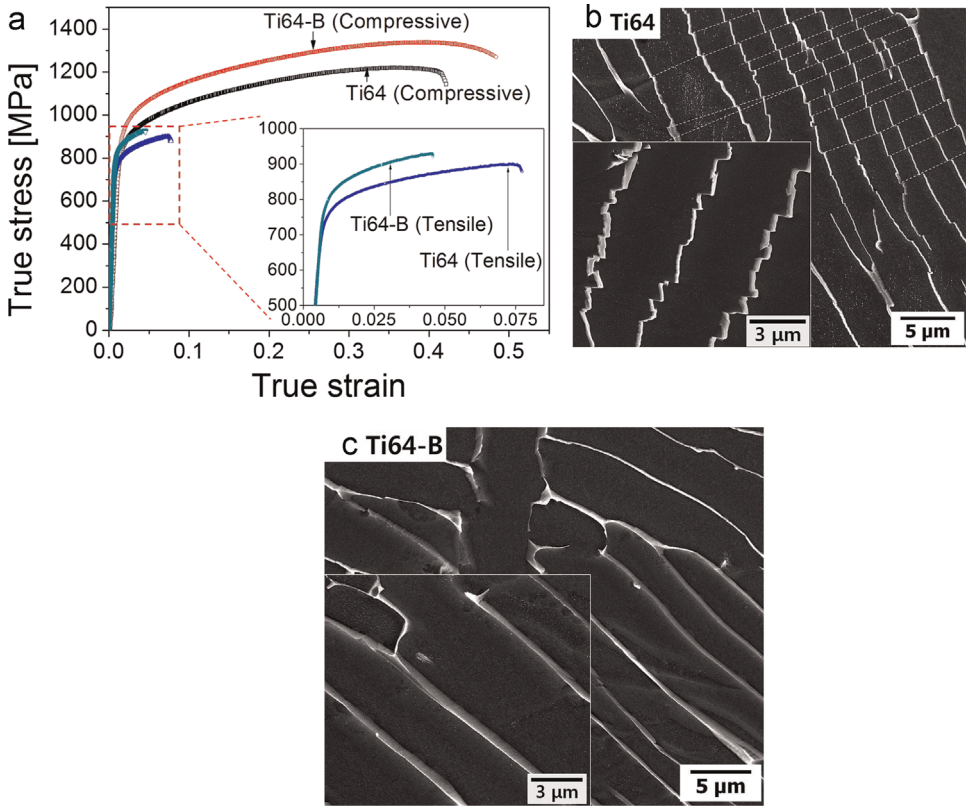

Fig. 2. Results of uniaxial tests; (a) tensile and compressive stress–strain curves of Ti64 and Ti64-B (with inset showing the enlarged tensile curve); (b) post-compression microstructure of Ti64 and (c) that of Ti64-B.

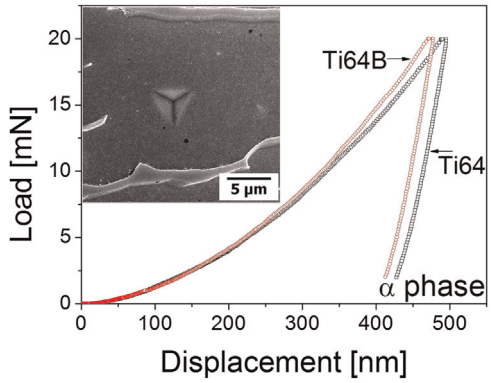

Fig. 3. Representative *P*–*h* curves for α phase (with inset image showing hardness impression made within the phase).

during nanoindentation on the α phase in Ti64 and Ti64-B. It is evident that α phase of Ti64 exhibits a larger peak-load displacement (h_{max}) compared to that made on α phase of Ti64-B. This implies that α phase in Ti64 is softer than that in Ti64-B. Note that the indentations were first made on the electro-polished mirror surfaces. To reveal the locations within the microstructure where the indents are made, the indented surfaces were gently etched and observed in an SEM. Then, the indentations made well within the target phase were considered as the representative of that constituent phase and were selected for analysis (see the inset image of Fig. 3).

From the experimentally measured hardness values of α phase, H_α, and the overall region that includes both α and β phases, $H_{\alpha\text{-}\beta}$, which is assumed to be determined by a simple rule-of-mixture, the hardness of β phase, H_β, is estimated as

$$H_\beta = \left(H_{\alpha-\beta} - H_\alpha f_\alpha\right)/f_\beta \tag{1}$$

where f is the volume fraction whose subscript represent the respective phases. It should be noted that the experimentally measured H values of α phase (from *P*–*h* curves in Fig. 3), $H_{\alpha,\mathrm{exp}}$, cannot be directly used as H_α of Eq. (1). This is because in this study $H_{\alpha\text{-}\beta}$ values of Eq. (1) were estimated from high-load nanoindentations (at 500 mN) whereas $H_{\alpha,\mathrm{exp}}$ values were obtained at 20 mN (see Fig. 3). Therefore, $H_{\alpha,\mathrm{exp}}$ and $H_{\alpha\text{-}\beta}$ cannot be directly compared to each other due to possible the indentation size effect (ISE), i.e. an increase in H with decreasing h for a sharp indenter [20]. To take ISE into account, the following Nix–Gao equation has been used [20]:

$$H_\alpha = H_{\alpha,\mathrm{exp}}\left(\sqrt{1+\frac{h^*}{h}}\right)^{-1} \tag{2}$$

where h^* is a material length scale for h-dependent H_α. The values of both H_α and h^* can be extracted by fitting the $H_{\alpha,\mathrm{exp}}$ (the average hardness data obtained through the CSM mode indentation) and h data to Eq. (2). To determine f of each phase within the indentation-induced plastic zone, specific regions (near a reference mark) were imaged before (Fig. 4a) and after nanoindentation tests (Fig. 4b). For the sake of simplicity, the area of the plastic zone was assumed to be the same as that of the circle passing three (or at least two) angular points of the triangular hardness impression. An example of the image taken using an image analyzer is also provided in the inset black–white image where the black and white areas correspond to α and β phases, respectively. The value of f_β can be calculated from such an image (e.g., f_β=0.105 for the inset of Fig. 4b), and f_α can be also simply determined as $(1-f_\beta)$.

The above procedure gives H_α values as 4.11 ± 0.016 and 4.36 ± 0.024 GPa (the standard deviations are also obtained by fitting the $H_{\alpha,\mathrm{exp}}$ and h data to Eq. (2)) for Ti64 and Ti64-B

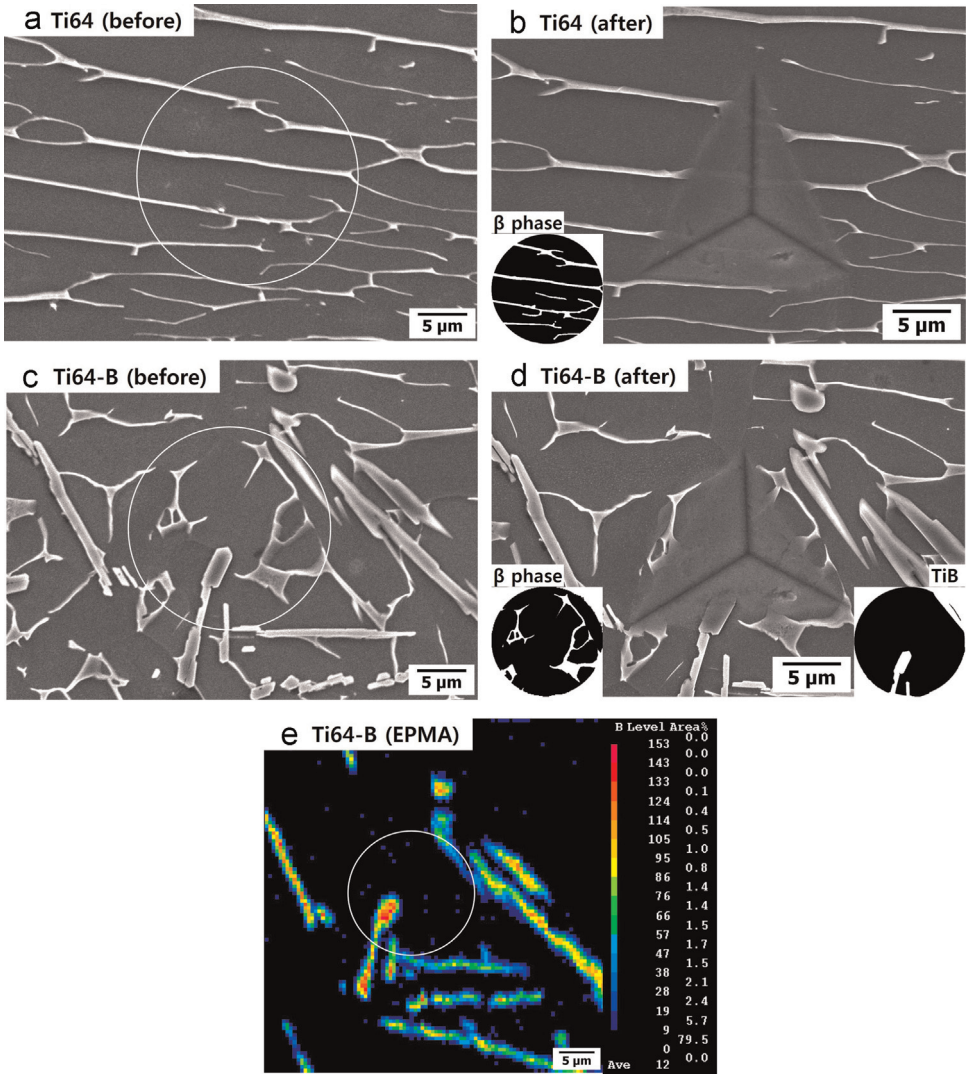

Fig. 4. Estimation of volume fraction within indentation-induced plastic zone: Scanning electron micrographs taken before [(a),(c)] and after [(b),(d)] high-load nanoindentation tests at 500mN; (a) and (b) for Ti64, and (c) and (d) for Ti64-B; (e) compositional maps from EPMA analysis of B distribution for the same region as (d).

respectively, both of which are in reasonable agreement with literature data [21]. Thus the enhancement in the hardness of the α phase due to B addition, ΔH_{α}, is ~250 MPa. Assuming further the constraint factor, C, in Tabor's empirical relation, $\sigma = H/C$, that connects flow stress, σ, to H, as 3, the enhancement in flow stress, $\Delta\sigma$, of α due to B addition ~83 MPa. Note that this increase is exclusively due to the refinement in the relevant microstructural length scale, namely the α-β colony size, and not due to solid solution strengthening as the solubility of B in α phase is extremely small (0.0004 wt%) [22]. Therefore, it is reasonable to conclude that the strengthening of α phase is mainly due to reduction in the effective slip length, which was discussed above, rather than solid solution strengthening and/or precipitation strengthening effect caused by the TiB particles.

By substituting the measured data of H_{α}, $H_{\alpha\text{-}\beta}$, and f_{α} into Eq. (1), H_{β} of Ti64 was estimated as 5.55 ± 0.23 GPa, which is much higher (by about 1 GPa) than H_{α}, supporting the notion that the plastic deformation within the α phase in Ti64-B may be constrained by surrounding β phase that is considerably harder. Interestingly, the estimated value of H_{β} in Ti64-B, made from the nanoindentations made at regions without TiB precipitates, is 5.61 ± 0.28 GPa, i.e., only ~1% higher than that measured in Ti64. Such small or no difference in hardness values of β phases in Ti64 and Ti64-B implies that strength of β phase does not change with the B addition.

As noted earlier, uniaxial compression tests indicate that the strength enhancement due to B addition, $\Delta\sigma$, of ~120 MPa. Out of this, ~83 MPa is due to microstructural refinement. Therefore, the remaining strength enhancement, which is about 40 MPa, still needs to be accounted for. We presume that it is possibly due to strengthening caused by the TiB particles. In Ti64-B alloy, these particles are generally located at the prior β grain boundaries, forming a necklace-like arrangement. Due to the large size of the TiB particles (20–100 μm) and their nature as a hard ceramic phase, composite-like strengthening (rather than precipitation hardening) can be expected from it [23]. To examine this, the hardness of the TiB, H_{TiB}, was estimated through the rule-of-mixture analysis of the nanoindentations made at the regions including all three phases of α, β, and TiB. Similar to the procedure described above and elsewhere [24–26], the SEM images were taken before (Fig. 4c) and after nanoindentation (Fig. 4d) and the f of each phase within the plastic zone (approximate) was calculated. To make sure that the analyzed target phase is TiB (not β), EPMA experiments were performed at selected cases. An example of EPMA compositional maps (for B) is exhibited in Fig. 4e showing a good match with inset image of TiB in Fig. 4d. The computed H_{TiB} was 21.49 ± 2.04 GPa which agrees well with literature data [21, 27]. Despite of the fact that the average volume fraction of TiB, f_{TiB},

in the examined Ti64-B is only ~2% [9], one can expect a finite contribution from it to the strength enhancement, especially since H_{TiB} is much higher than both H_α and H_β. In the following, we make an approximate estimation of it.

The average volume fraction of each constituent phase was determined through SEM observations. While average value of f_α and f_β in Ti64 is ~0.88 and ~0.12 respectively, f_α, f_β, and f_{TiB} in Ti64-B is ~0.88, ~0.1, and ~0.02 respectively. With these fraction values, the values of H_α, H_β, and H_{TiB} were put into a simple rule-of-mixture equation (i.e., overall hardness of a composite having n phases, $H_{overall} = \sum_{i=1}^{n} f_i H_i$), resulting in the H_{overall} value of ~4.3 and ~4.8 GPa for Ti64 and Ti64-B, respectively. Hence the estimated $\Delta H_{\mathrm{overall}}$ is ~0.5 GPa and, by Tabor's relation, $\Delta\sigma$ is ~167 MPa, which is higher than that observed in the compression test results. However, large variance in f_{TiB} from location to location within the microstructure is observed, with a non-negligible standard deviation of as much as 0.005 [9]. Therefore, the estimated $\Delta\sigma$ can be assumed to be reasonably close to the experimental $\Delta\sigma$ (~120 MPa) from compression tests, which supports that the suggested strengthening mechanism holds.

4. Summary

In summary, an attempt was made to examine the relative contributions of various strengthening mechanisms to the enhanced flow strength of a Ti–6Al–4V alloy modified by the addition of B in a small quantity. This was accomplished by conducting nanoindentation experiments on various constituent phases in the microstructure and analysis of the results to decouple of the individual contributions to overall strength of the alloy. Our results suggest that two independent mechanisms contribute to observed strengthening of B-modified alloys; one is the strengthening of α phase (matrix phase) by the decrease in the effective slip length, and the other is the composite strengthening effect by TiB particles. Validity of this suggestion was discussed based on rule-of-mixture analysis with phase hardness.

Acknowledgments

The work at Hanyang University was supported in part by the National Research Foundation of Korea (NRF) Grant funded by the Korea government (MSIP) (No. 2013R1A1A2A10058551), and in part by the Human Resources Development program of the Korea Institute of Energy Technology Evaluation and Planning (KETEP) Grant funded by the Korea government (MOTIE) (No. 20134030200360). The work at King Abdulaziz University (KAU) was funded through a project by the Deanship of Scientific Research (DSR), under Grant no. (16-130-35-HiCi). The authors from KAU, therefore, acknowledge technical and financial support of KAU."

References

[1] G. Welsch, R. Boyer, E.W. Collings, Materials Properties Handbook: Titanium Alloys, ASM international, Ohio, 1993.
[2] R.R. Boyer, Mater. Sci. Eng. A 213 (1996) 103–114.
[3] W.G. Burgers, Physica 1 (1934) 561–586.
[4] G. Lutjering, Mater. Sci. Eng. A 243 (1998) 32–45.
[5] G. Lütjering, J.C. Williams, Titanium: Engineering Materials and Processes, Second ed., Springer, Berlin, 2007.
[6] M.G. Glavicic, P.A. Kobryn, F. Spadafora, S.L. Semiatin, Mater. Sci. Eng. A 346 (2003) 8–18.
[7] S. Tamirisakandala, R.B. Bhat, 53, 2005, pp. 1421–1426.
[8] I. Sen, S. Tamirisakandala, D.B. Miracle, U. Ramamurty, Acta Mater. 55 (2007) 4983–4993.
[9] I. Sen, K. Gopinath, R. Datta, U. Ramamurty, Acta Mater. 58 (2010) 6799–6809.
[10] I. Sen, U. Ramamurty, Scr. Mater. 62 (2010) 37–40.
[11] G. Singh, I. Sen, K. Gopinath, U. Ramamurty, Mater. Sci. Eng. A 540 (2012) 142–151.
[12] G. Singh, R. Gaddam, V. Petley, R. Datta, R. Pederson, U. Ramamurty, Scr. Mater. 69 (2013) 698–701.
[13] G. Singh, D.V.V. Satyanarayana, R. Pederson, R. Datta, U. Ramamurty, Mater. Sci. Eng. A 597 (2014) 194–203.
[14] S. Tamirisakandala, D.B. Miracle, Int. J. Adv. Eng. Sci. Appl. Math. 2 (2010) 168–180.
[15] W.C. Oliver, G.M. Pharr, J. Mater. Res. 7 (1992) 1564–1583.
[16] X. Feaugas, M. Clavel, Acta Mater. 45 (1997) 2685–2701.
[17] T. Neeraj, D.-H. Hou, G.S. Daehn, M.J. Mills, Acta Mater. 48 (2000) 1225–1238.
[18] J.C. Williams, A.W. Sommer, P.P. Tung, Metall. Trans. 3 (1972) 2979–2984.
[19] T. Neeraj, M.J. Mills, Mater. Sci. Eng. A 319–321 (2001) 415–419.
[20] G.M. Pharr, E.G. Herbert, Y. Gao, Annu. Rev. Mater. Res. 40 (2010) 271–292.
[21] M.J. Bermingham, D. Kent, H. Zhan, D.H. StJohn, M.S. Dargusch, Acta Mater. 91 (2015) 289–303.
[22] J.R. Murray, P.K. Liao, K.E. Spear, Bull. Alloy. Phase Diag. 7 (1986) 550–555.
[23] C.J. Boehlert, S. Tamirisakandala, W.A. Curtin, D.B. Miracle, Scr. Mater. 61 (2009) 245–248.
[24] B.-W. Choi, D.-H. Seo, J.-i. Jang, Met. Mater. Int. 15 (2009) 373–378.
[25] M.-Y. Seok, Y.-J. Kim, I.-C. Choi, Y. Zhao, J.-i. Jang, Int. J. Plast. 59 (2014) 108–118.
[26] M.-Y. Seok, I.-C. Choi, J. Moon, S. Kim, U. Ramamurty, J.-i. Jang, Scripta Mater. 87 (2014) 49–52.
[27] R. Barnerjee, A. Genc, P.C. Collins, H.L. Fraser, Metall. Mater. Trans. A 35A (2004) 2143–2152.